Available online at www.sciencedirect.com

SciVerse ScienceDirect

Ceramics International 38 (2012) 6739–6751

CERAMICS INTERNATIONAL

www.elsevier.com/locate/ceramint

Synthesis of $CuGa_2O_4$ nanoparticles by precursor and self-propagating combustion methods

Dana Gingasu[a], Ioana Mindru[a,*], Luminita Patron[a], Gabriela Marinescu[a], Floriana Tuna[a,b], Silviu Preda[a], Jose Maria Calderon-Moreno[a], Cristian Andronescu[a]

[a]*Ilie Murgulescu Institute of Physical Chemistry, Romanian Academy, Splaiul Independentei 202, Bucharest 060021, Romania*
[b]*School of Chemistry, University of Manchester, Oxford Road, M13 9PL Manchester, UK*

Received 19 March 2012; received in revised form 22 May 2012; accepted 22 May 2012
Available online 31 May 2012

Abstract

Copper gallate spinels, $CuGa_2O_4$, have been synthesized by two wet chemical routes: precursor method and self-propagating combustion involving a glycine-nitrate system. All complex precursors have been characterized by chemical analysis, infrared spectroscopy (IR), ultraviolet visible spectroscopy (UV–vis), electron paramagnetic resonance spectroscopy (EPR), thermal analysis and scanning electron microscopy (SEM). The copper gallate spinel oxides have been further investigated by X-ray diffraction (XRD), SEM, IR, UV–vis, magnetic measurements and EPR. The crystallite size of the copper gallate was found about 280 Å.

Keywords: A. Powders: chemical preparation; B. Spectroscopy; D. Spinels; X-ray diffraction

1. Introduction

Cu-based spinel oxides CuB_2O_4 ($B^{3+}=Fe^{3+}$, Cr^{3+}, Ga^{3+}, Al^{3+}) have attracted interest from the viewpoint of their technical applications. They are recognized as active catalysts for steam reforming of dimethyl-ether (DME)—a promising hydrogen source [1], as well as photocatalysts for solar hydrogen production [2]. The sensing behavior of MGa_2O_4 ($M^{2+}=Zn^{2+}$, $Cd^{2+}_{1-x}Zn^{2+}_x$, Cu^{2+}) towards inflammable and toxic gases [3–5] is also well-known. However, literature reports concerning synthesis, physicochemical properties and structural characteristics of transition metal gallates (MGa_2O_4 where $M^{2+}=Mg^{2+}$, Zn^{2+}, Cu^{2+}, etc.) are rather scarce.

Generally, control over particle size, surface area and crystallinity is indispensable to develop catalytic and photocatalytic properties [6]. The most common synthetic routes for obtaining such oxides are (i) solid-state reactions [2,7–9], (ii) chemical methods including microwave-hydrothermal [6,10,11] and sol–gel synthesis [1,12], and (iii) complexation method [5,13].

The present paper reports on the obtaining of $CuGa_2O_4$ by two wet chemical routes: (i) *precursor method* which means complexation followed by thermal decomposition of the resulting polynuclear complexes and (ii) *self-propagating combustion* using a glycine-nitrate system.

The goal of this study was to synthesize polynuclear coordination compounds, precursors of copper gallate, containing as ligands the anions of tartaric acid, gluconic acid or glycine and to characterize these complex compounds by chemical analysis, IR, UV–vis, EPR and SEM; to separate the complex compounds from the precursor solution used in self-propagating combustion (glycine nitrate process-GNP) and to characterize them by chemical analysis, IR and UV–vis spectroscopy; to study the thermal decomposition of all compounds in order to obtain copper gallates and to characterize these samples by XRD, SEM, IR, UV–vis and EPR spectroscopy.

*Corresponding author. Tel.: +40 021 316 79 12; fax: +40 021 312 11 47.
E-mail address: imandru@yahoo.com (I. Mindru).

0272-8842/$36.00
http://dx.doi.org/10.1016/j.ceramint.2012.05.067

2. Experimental

2.1. Reagents

All chemicals: $Ga(NO_3)_3 \cdot 9H_2O$, $Cu(NO_3)_2 \cdot 3H_2O$, tartaric acid ($C_4O_6H_6$), δ-gluconolactone ($C_6H_{10}O_6$) and glycine (NH_2CH_2COOH) were of reagent quality (Merck).

2.2. $CuGa_2O_4$ preparation

2.2.1. Complexation method

For the synthesis of complex precursors, the following systems were studied:

$2Ga(NO_3)_3 \cdot 9H_2O{:}1Cu(NO_3)_2 \cdot 3H_2O{:}4C_4O_6H_4^{2-}$

$2Ga(NO_3)_3 \cdot 9H_2O{:}1Cu(NO_3)_2 \cdot 3H_2O{:}8C_6O_7H_{11}^{-}$

$2Ga(NO_3)_3 \cdot 9H_2O{:}1Cu(NO_3)_2 \cdot 3H_2O{:}8NH_2CH_2COOH$

Gallium and copper nitrates were dissolved in the minimum amount of water and mixed with an aqueous solution of tartarate acid in a 2:1:4 (cations/tartaric acid) ratio, 2:1:8 (cations/δ-gluconolactone) ratio (δ-gluconolactone converted into gluconic acid by hydrolysis at 80 °C) and 2:1:8 (cations/glycine). Ethanol was added to the final solution until a blue precipitate was formed. The pH was raised to 6 by adding NH_4OH:ethanol (1:1). After 24 h at 4 °C, the precipitate was filtered and dried over P_4O_{10}.

The results of the chemical analysis for the precursors are reported in Table 1.

In order to prepare well-crystallized copper gallate oxides, these complex precursors were calcined at 1000 °C for 1 h.

2.2.2. Self-propagating combustion

Another investigated system was

$2Ga(NO_3)_3 \cdot 9H_2O{:}1Cu(NO_3)_2 \cdot 3H_2O{:}4.5NH_2CH_2COOH$

This system was used to obtain the precursor concentrate solution for self-combustion reaction.

The equivalence ratio, (φe = oxidizer/fuel) of the redox mixture for the combustion is calculated by using the total oxidizing and reducing valencies of the oxidizer and of the fuel which serve as numerical coefficients, so that φe becomes unity and the heat released is at its maximum [14–16]. According to the principles used in propellant chemistry, the oxidizing and reducing valencies of various elements are considered as follows: C = 4, H = 1, O = −2, N = 0, $M^{2+} = 2$, $M^{3+} = 3$, etc.

Thus, the oxidizing valency of $Cu(NO_3)_2$ becomes (−10); for $Ga(NO_3)_3$, it is (−15), which should be balanced by the total valencies in the fuel; glycine (H_2NCH_2COOH), which add up to (+9). Therefore, the molar proportion of the oxidizing metal nitrates and reducing fuel (glycine) is $Ga(NO_3)_3$:$Cu(NO_3)_2$:glycine = 2:1:4.5.

The nitrates and glycine were mixed in an agate mortar till a concentrate homogeneous solution was formed. The solvent is the water hydration of nitrates, only. This solution is placed on P_4O_{10}. By dehydration, after 48 h, a blue compound (**IV**) was obtained (Table 1).

The possible chemical reaction assuming complete combustion can be written as follows:

$$18Ga(NO_3)_3 + 9Cu(NO_3)_2 + 40NH_2CH_2COOH = 9CuGa_2O_4 + 80CO_2 + 100H_2O + 56N_2$$

The as-burnt powder was calcined at 1000 °C for 1 h.

2.3. Characterization techniques

The metal content of the complex compounds was determined by atomic absorption spectroscopy with an SAA1 instrument and by gravimetric techniques; the C, N and H values were obtained using a Carbo Erba Model 1108 CHNSO elemental analyzer.

The IR spectra of the polynuclear coordination compounds and spinel gallates were recorded on KBr pellets with a JASCO FTIR 4100 spectrophotometer in the 4000–400 cm^{-1} range.

Absorption measurements were made with the JASCO V-670 spectrophotometer.

Electron paramagnetic resonance (EPR) measurements were performed on powder samples at 5 and 298 K, with a Bruker EMX spectrometer working at X-band (9.4 GHz) microwave frequency and 100 kHz field modulation. Experiments at 5 K were carried under liquid helium using an Oxford Instruments cryostat. EPR parameters were determined by simulating the spectra using a Bruker Simfonia software package.

Table 1
Chemical analysis of precursors.

Precursor	Ga (wt%)		Cu (wt%)		C (wt%)		N (wt%)		H (wt%)	
	Calcd.	Found	Calcd.	Found	Calcd.	Found	Calcd.	Found	Calcd.	Found
I	13.60	13.88	6.20	6.29	18.73	18.80	5.46	5.29	4.48	4.41
II	12.24	12.09	5.58	5.64	25.28	25.34	2.46	2.22	5.27	5.42
III	18.45	18.28	8.40	8.32	12.69	12.31	9.26	9.37	4.63	4.53
IV	12.19	12.30	5.55	5.65	9.44	9.50	15.30	15.40	3.02	3.10

I = $(NH_4)_4[CuGa_2(C_4O_6H_4)_4(OH)_4] \cdot 5H_2O$; **II** = $(NH_4)_2[CuGa_2(C_6O_7H_{11})_4(OH)_6] \cdot H_2O$; **III** = $[CuGa_2(NH_2CH_2COO)_4(OH)_3](NO_3) \cdot 8H_2O$; **IV** = $[CuGa_2(NH_2CH_2COOH)_{4.5}](NO_3)_8 \cdot 6H_2O$.

Thermal measurements (TG, DTG and DTA) were performed using a Mettler Toledo TGA-SDTA 851 equipment in an air static atmosphere. The measurements were carried out in the range of 25–1000 °C with 10 °C min^{-1} heating rate.

X-ray diffraction data were collected using parallel beam geometry on Rigaku's Ultima IV X-ray powder diffractometer, with CuKα radiation ($\lambda = 1.54$ Å), CBO optics, operating at 40 kV and 30 mA, 0.02° step size and 5° /min. scan speed. Phase identification and Rietveld analysis were performed using Rigaku's PDXL software, with Whole Pattern Fitting (WPF) module, connected to ICDD PDF-2 database.

The surface morphology was investigated without further sample preparation prior to observation, on as-prepared powders calcined at 1000 °C for 1 h, by Scanning Electron Microscopy (SEM) using a Zeiss EVO LS10 environmental microscope working at 20 kV, the power calcined at 700 °C and the complex precursors were observed in a FEI Quanta 3D FEG microscope, operating at 20 kV, equipped with an energy dispersive X-ray (EDX) spectrometer.

The magnetic measurements on the copper gallate samples are performed with a Faraday balance ($HgCo(SCN)_4$, $\chi_g = 16.44 \times 10^{-6}$ cgs units and metallic Ni as calibrants).

3. Results and discussion

3.1. Characterization of $CuGa_2O_4$ precursors

The concept of *chimie douce* (wet chemistry) was introduced by Livage [17–19]. This concept had open the way for the construction of multitude inorganic and hybrid organic–inorganic nanomaterials [20].

The *precursor method* (known also as the *complexation method*) and *self-propagating combustion* are two chemical synthetic routes belonging to *chimie douce* in which polynuclear coordination compounds with two or more metal ions are formed as complex precursors.

Generally, the complexing agents used in the first method are chelating agents which contain carboxyl and/or amine groups. In our research tartaric acid, gluconic acid and glycine have been chosen. It is known that glycine acts as a complexing agent for a number of metal ions, containing both a carboxylic acid group and an amino group and, also, it is a very good fuel for the combustion reaction being oxidized by nitrate ions (GNP-glycine process).

The complex precursors (**I**–**IV**) were characterized by IR, UV–vis, EPR and thermal analysis.

3.1.1. Infrared spectra

$(NH_4)_4[CuGa_2(C_4O_6H_4)_4(OH)_4] \cdot 5H_2O$ **I**. The IR spectrum of tartaric acid shows a band at 1740 cm^{-1} assigned to the ν(CO) vibration. After the formation of the coordination compound, this band disappears and it is replaced by two intensive bands: ν_{asym}(OCO) (1638 cm^{-1}) and ν_{sym}(OCO) (1396 cm^{-1}) (Fig. 1a).

On the basis of spectroscopic criteria [21], the magnitude of the separation $\Delta\nu = \nu_{asym} - \nu_{sym}$ may be an indicative of the coordination mode of carboxylate anions. From the IR spectrum of the tartarate compound, $\Delta\nu$ is 242 cm^{-1}, being comparable with the value of 240 cm^{-1} in sodium tartarate; this indicates bridging bonding coordination for the COO^- groups. In the tartaric acid spectrum, the peak at ~1090 cm^{-1} is assigned to C–O stretching vibration of the OH secondary groups. In the spectrum of $(NH_4)_4[CuGa_2(C_4O_6H_4)_4(OH)_4] \cdot 5H_2O$, this band splits and shifts toward lower frequencies (1070–1000 cm^{-1}). Such splitting can be explained by dissimilar bonding of the OH secondary groups to two different metal ions.

The tartarate compound also exhibits a broad and intensive band in the 3000–3500 cm^{-1} range. This band can be assigned to the vibrations of water molecules/the formation of hydrogen bonds between water and/or hydroxyl groups.

$(NH_4)_2[CuGa_2(C_6O_7H_{11})_4(OH)_6] \cdot H_2O$ **II**. The IR spectrum of the gluconate compound evidences two strong bands located at 1636 cm^{-1} (ν_{asym}OCO) and at 1398 cm^{-1} (ν_{sym}OCO) assigned to coordinated COO^- groups (Fig. 1b). Comparison of this spectrum with that of the free acid shows a shift of the doublet bands from 1100–1090 cm^{-1} towards smaller values (~1090, ~1050 cm^{-1}), consistent with coordination through one or several OH groups. The gluconate compound exhibits a broad, very intensive band in the 3000–3500 cm^{-1} (with maximum ~3379 cm^{-1}) range which can be assigned to the vibration of water molecules/the formation of hydrogen bonds between water and/or hydroxyl groups.

$[CuGa_2(NH_2CH_2COO)_4(OH)_3]NO_3 \cdot 8H_2O$ **III**. The IR spectrum of this compound (Fig. 1c) suggests that glycine acts as a monodentate ligand (ν_{asym}OCO at ~1607 cm^{-1} and ν_{sym}OCO at ~1385 cm^{-1}). A band characteristic of the OH^- ion vibration is also present as a dissimilar peak (~3264 cm^{-1}) on the broad intensive band due to the vibration of water molecule.

$[CuGa_2(NH_2CH_2COOH)_{4.5}](NO_3)_8 \cdot 6H_2O$ **IV**. By comparison with the IR spectrum of compound **III**, the bands assigned to the coordinated carboxylic groups appear at ~1631 cm^{-1} (ν_{asym}OCO) and ~1346 cm^{-1} (ν_{sym}OCO) (Fig. 1d) which means that in this compound, glycine acts as a chelate ligand. Both IR spectra exhibit a very intensive, sharp band at ~1385 cm^{-1} which can be assigned to the NO_3^- ion [21].

3.1.2. UV–vis and EPR spectra

The UV–vis spectra of the complex precursors exhibit an asymmetric broad band assigned to d–d transitions, centered in the range 600–850 nm which corresponds to $^2T_{2g} \leftarrow {}^2E_g$, as expected for an octahedral distorted geometry of Cu(II) ions [22–25]. Charge transfer bands appear at ~300 nm (Fig. 2).

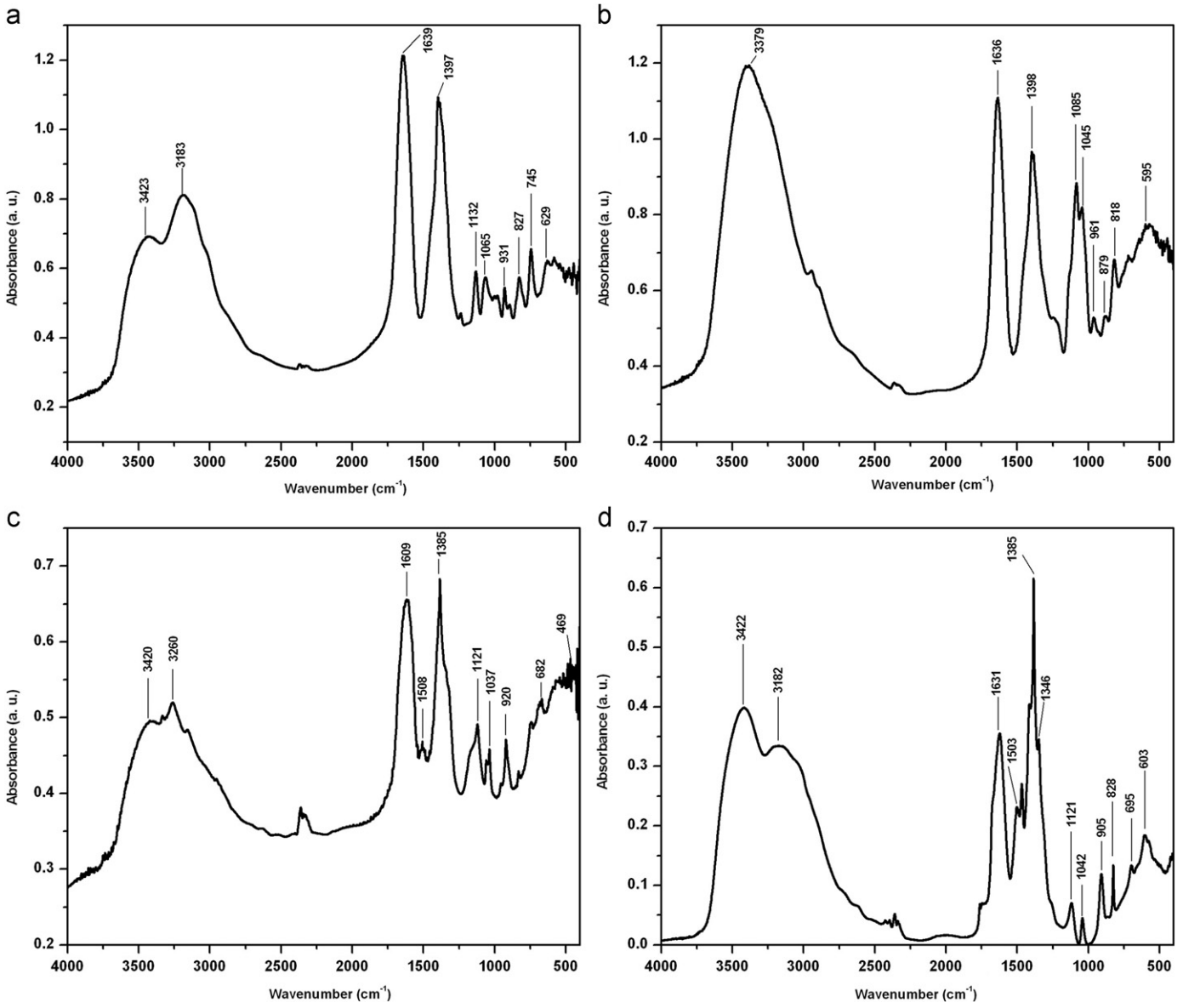

Fig. 1. IR spectra of (a) $(NH_4)_4[CuGa_2(C_4O_6H_4)_4(OH)_4]\cdot 5H_2O$; (b) $(NH_4)_2[CuGa_2(C_6O_7H_{11})_4(OH)_6]\cdot H_2O$; (c) $[CuGa_2(NH_2CH_2COO)_4(OH)_3]NO_3\cdot 8H_2O$ and (d) $[CuGa_2(NH_2CH_2COOH)_{4.5}](NO_3)_8\cdot 6H_2O$.

The room temperature X-band EPR spectrum of $(NH_4)_2[CuGa_2(C_6O_7H_{11})_4(OH)_6]\cdot H_2O$ is typical to the axial symmetry (Fig. 3). It indicates the presence of a single type of Cu-centers with $g_{II}=2.31$, $g_{\perp}=2.11$, $A_{II}=150$ G and $A_{\perp}=50$ G. Such large values of g_{II} and A_{II} suggest that the coordination geometry of Cu(II) is an elongated distorted octahedron with the unpaired electron occupying the $3d_{x^2-y^2}$ orbital (Table 2) [25,26]. The EPR spectrum at 5 K resembles that recorded at 298 K, suggesting that the geometry around Cu(II) is preserved at low temperatures. Simulation of this spectrum gave $g_{II}=2.31$, $g_{\perp}=2.10$, $A_{II}=155$ G and $A_{\perp}=50$ G (Fig. 3). It has been reported that high g_{II} values are common for six coordinate Cu(II) complexes with oxygen-containing ligands [27,28].

The g values are related by the expression:

$$G=\frac{g_{II}-2}{g_{\perp}-2}$$

which is a measure of exchange interaction between the Cu centers in the compound [27,29]. If $G>4$ the interaction is negligible; if $G<4$ considerable exchange interaction exists in this compound. For the compound $(NH_4)_2[CuGa_2(C_6O_7H_{11})_4(OH)_6]\cdot H_2O$, $G\sim 2.82$ indicates an exchange interaction.

3.1.3. Thermal decomposition

In order to establish the optimal conditions for the conversion of the polynuclear compounds into copper

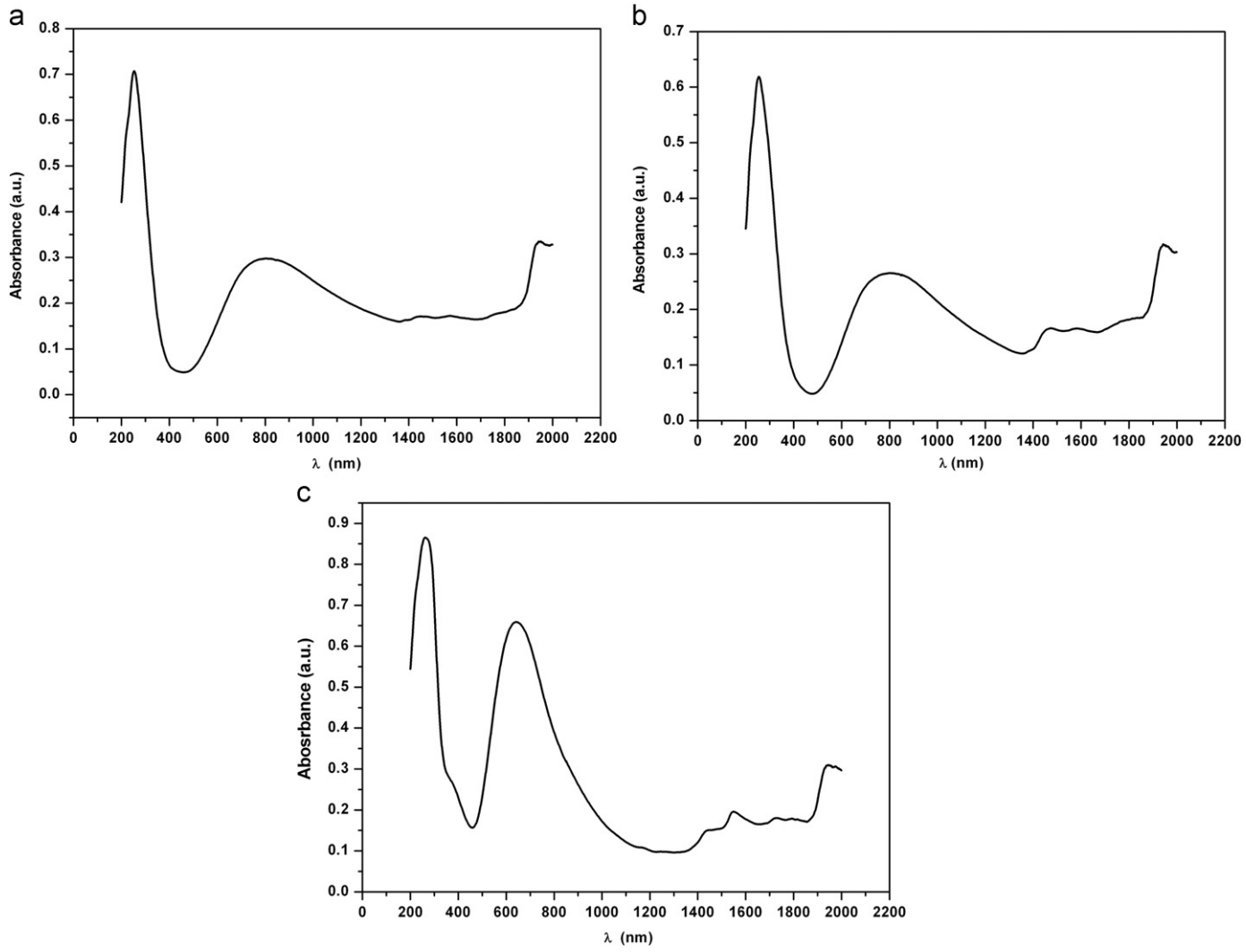

Fig. 2. UV–vis spectra of (a) $(NH_4)_4[CuGa_2(C_4O_6H_4)_4(OH)_4]\cdot 5H_2O$; (b) $(NH_4)_2[CuGa_2(C_6O_7H_{11})_4(OH)_6]\cdot H_2O$ and (c) $[CuGa_2(NH_2CH_2COO)_4(OH)_3]NO_3\cdot 8H_2O$.

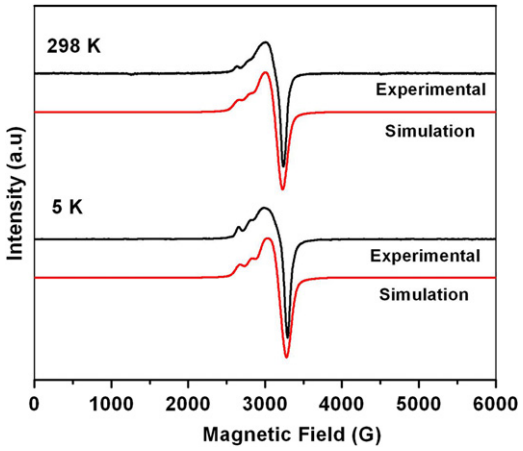

Fig. 3. X-band EPR spectra of $(NH_4)_2[CuGa_2(C_6O_7H_{11})_4(OH)_6]\cdot H_2O$.

gallate, their thermal decompositions were investigated. The thermal behaviors of the multimetallic compounds are presented in Fig. 4.

The weight loss below 170 °C associated with endothermic DTA peak arises from the loss of adsorbed water for all of these compounds. The exothermic sharp peak in DTA curves which ranges between 285 °C (compound **I**) and 187 °C (compound **IV**) accompanied by a very large weight loss (~50 wt%) in TG curves is caused by the decomposition of the complex precursors and evolution of large amounts of gases, such as CO, CO_2, NO_2 and H_2O.

It is very interesting to compare the thermal decomposition of complex compounds containing glycine as ligands (**III** and **IV**) (Fig. 4c and d).

A gradual decomposition through three steps is recorded for $[CuGa_2(NH_2CH_2COO)_4(OH)_3]NO_3\cdot 8H_2O$ **III** with the exothermic peak at ~226 °C, unlike the decomposition of the compound $[CuGa_2(NH_2CH_2COOH)_{4.5}](NO_3)_8\cdot 6H_2O$ **IV** which occurs in two steps. The exothermic peak in DTA curve, at ~187 °C (a temperature smaller than that recorded for compound **III**) is very sharp and sustains a self-combustion process for the last compound.

Table 2
EPR data for complex and copper-gallium oxides (powder X-band EPR).

Experimental spectra	Theoretical spectra	$g_{xx}/g_{yy}/g_{zz}$	$A_{xx}/A_{yy}/A_{zz}$ (G)	$W_x/W_y/W_z$ (G)	L/G
Compound **II**	5 K-Sim RT-Sim	2.1/2.1/2.31 2.11/2.11/2.31	50/50/155 45/45/150	120/120/100 120/120/110	0.1 0.5
$CuGa_2O_4$ obtained by thermal decomposition of **I**	5 K-Sim RT-Sim	2.118/2.118/2.338 2.13/2.13/2.34	70/70/148 50/50/140	140/140/120 140/140/120	0.1 0.5
$CuGa_2O_4$ obtained by thermal decomposition of **II**	5 K-Sim RT-Sim	2.20/1.99/2.27 2.145/2.145/2.3	20/20/235 0/0/(0–20)	100/100/95 70/70/70	0.5 0.1

I=$(NH_4)_4[CuGa_2(C_4O_6H_4)_4(OH)_4]\cdot 5H_2O$; **II**=$(NH_4)_2[CuGa_2(C_6O_7H_{11})_4(OH)_6]\cdot H_2O$, RT=room temperature (298 K), A=hyperfine interaction, W=linewidth, L=Lorentzian shape, G=Gaussian shape (ex: 0.1 for Gaussian lines; 1 for Lorentz lines).

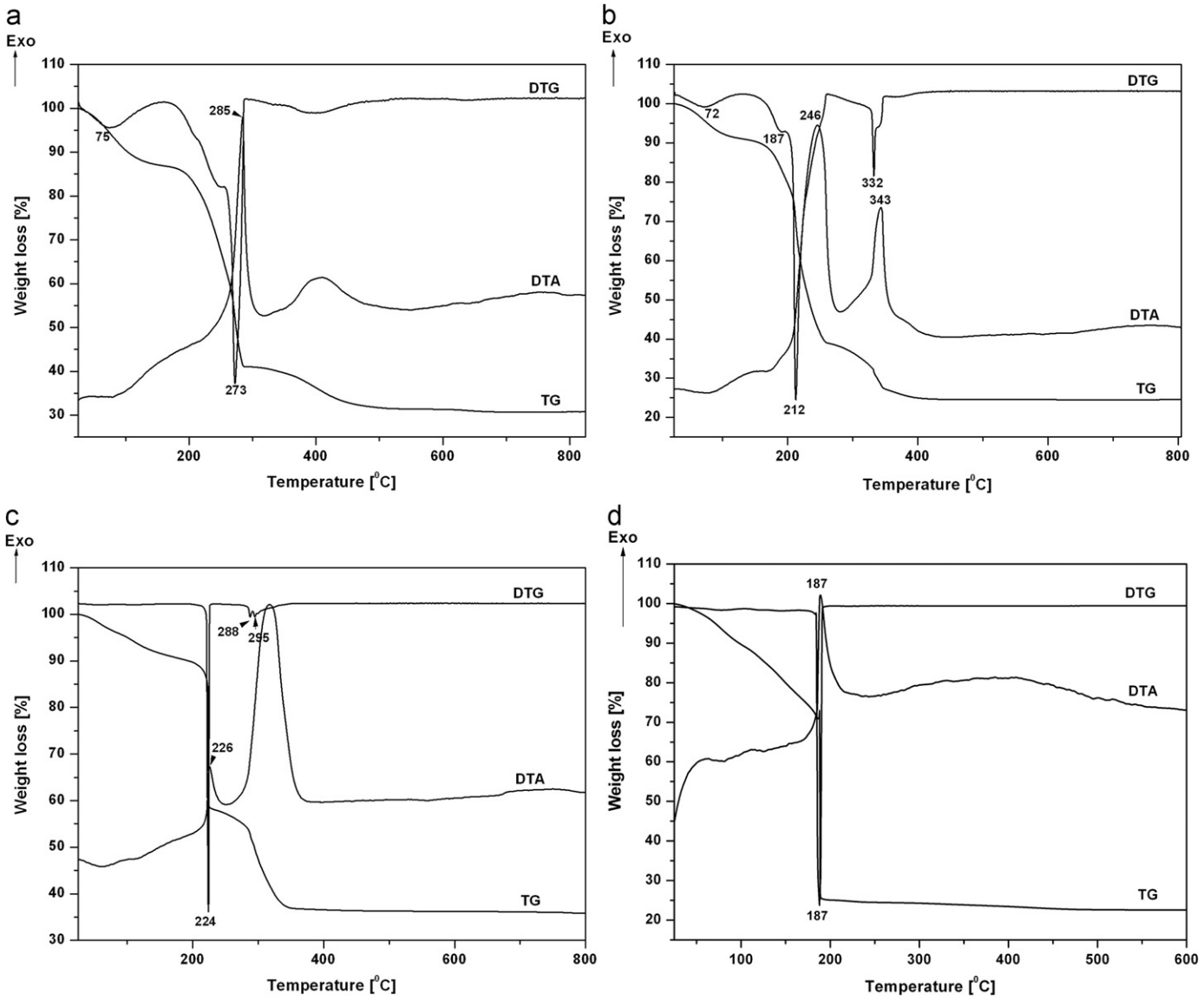

Fig. 4. TG, DTG and DTA curves of (a) $(NH_4)_4[CuGa_2(C_4O_6H_4)_4(OH)_4]\cdot 5H_2O$; (b) $(NH_4)_2[CuGa_2(C_6O_7H_{11})_4(OH)_6]\cdot H_2O$; (c) $[CuGa_2(NH_2CH_2COO)_4(OH)_3]NO_3\cdot 8H_2O$ and (d) $[CuGa_2(NH_2CH_2COOH)_{4.5}](NO_3)_8\cdot 6H_2O$.

The thermal decomposition of the polynuclear coordination compounds (**I–III**) showed in the temperature range of 400–600 °C that the process ends up with the formation of the oxidic phase.

SEM micrographs of the $CuGa_2O_4$ complex precursor compounds are shown in Fig. 5. Precursors **I** and **II** show a powder like morphology with particle size around 100–200 nm, while precursor **III** shows much coarser

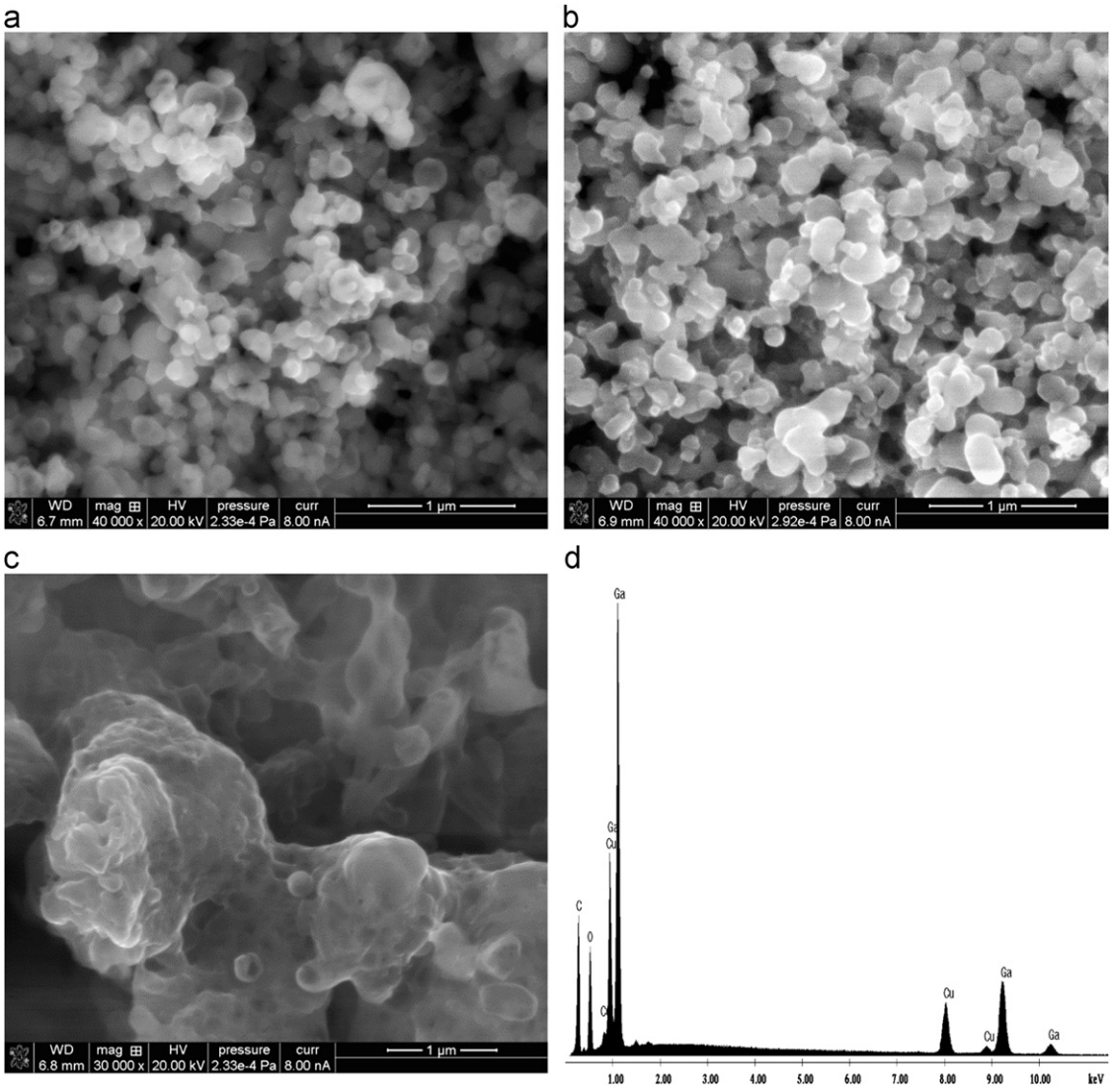

Fig. 5. SEM micrographs of complex precursors: (a) **I**; (b) **II**; (c) **III** and EDX spectrum of **II** (d).

agglomerates, and few non-aggregated fine particles. The EDX spectra detected the presence of C, N, O, Cu and Ga in all these precursors. The analysis from different areas in each sample demonstrated the homogeneous composition in each precursor and confirmed a ratio Cu:Ga of approximately 1:2. Fig. 5 shows a representative EDX spectrum of precursors **II**.

3.2. Characterization of $CuGa_2O_4$

All the copper gallate samples were characterized by means of XRD, SEM, UV–vis, magnetic measurements and EPR.

The X-ray diffraction patterns of $CuGa_2O_4$ powders obtained *via* precursor method and self-propagating combustion, calcined at 1000 °C/1 h, are presented in Fig. 6(a–d). The spinel gallate structure of $CuGa_2O_4$ (Fd3m), which was described in ICDD file number 00-044-0183 was detected in all four samples. Most of the peaks in the pattern from the oxide sample obtained by thermal decomposition of compound **III** (Fig. 6d) were assigned to $CuGa_2O_4$ with a spinel structure, but four extra peaks characteristic of CuO and Ga_2O_3 were also identified.

The calcination of compound **II** was conducted at two temperatures (700 °C and 1000 °C for 1 h) to observe the effect of the calcination temperature on the crystallization of $CuGa_2O_4$ powders (Fig. 6b). The XRD patterns for the sample calcined at 700 °C/1 h show identical diffraction patterns to those of the sample calcined at 1000 °C/1 h, but the diffraction peaks of $CuGa_2O_4$ phase become much sharper with the increase of calcination temperature, indicating the increasing of the crystallization process. Therefore, one can conclude that the optimized calcination temperature is 1000 °C.

Table 3 summarizes the lattice constant and the crystallite size for the copper gallate samples calcined at 1000 °C/1 h. The calculated lattice parameters matched closely to the standard lattice parameter value (8.30 Å). These values

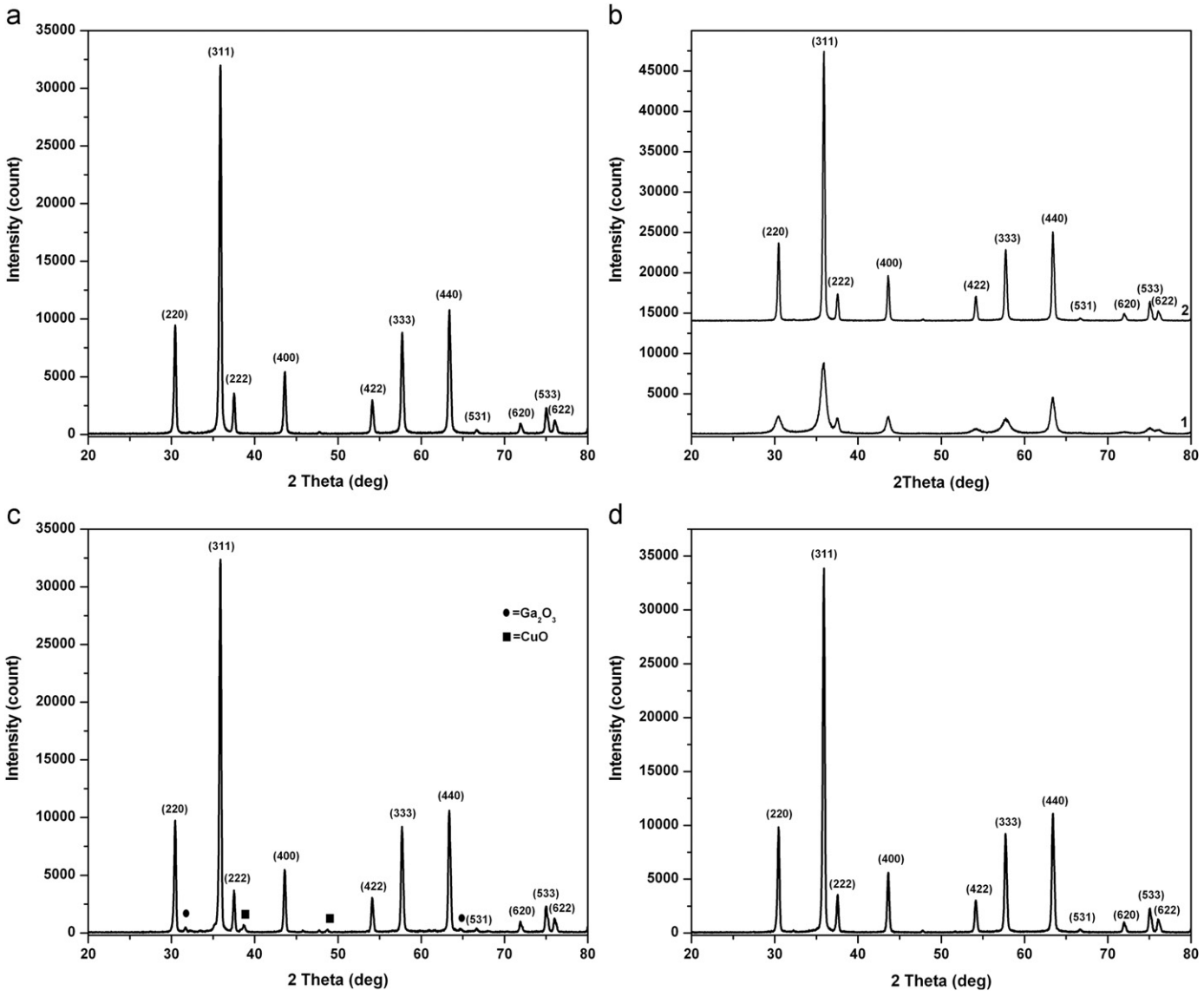

Fig. 6. XRD patterns of $CuGa_2O_4$ powders obtained from different complex precursors: (a) **I** calcined at 1000 °C/1 h; (b) **II** calcined at (1) 700 °C/1 h and (2) 1000 °C/1 h; (c) **III** calcined at 1000 °C/1 h and (d) **IV** calcined at 1000 °C/1 h.

are in good agreement with those reported in the literature [2,5]. The average crystallite size was found to be ~280 Å.

SEM micrographs of the $CuGa_2O_4$ powders obtained after thermal treatment at 1000 °C/1 h are shown in Fig. 7(a–f). Particles sized ~200 nm can be clearly observed in the powders obtained from the complex precursors **I** (Fig. 7a and e) and **IV** (Fig. 7d). According to the XRD results these particles are agglomerates of primary nanocrystallites. The SEM results indicate that thermal treatment necessary for the formation of well-crystallized $CuGa_2O_4$ powders results in partial sintering between adjacent grains. The formation of hard agglomerates of bigger size is clearly observed in the powder obtained from the complex precursor **III** (Fig. 7c and f). The higher magnification micrographs illustrated the different degrees of sintering of calcined powders from precursors **I** (Fig. 7e) and **III** (Fig. 7f). The morphology of $CuGa_2O_4$ powders (Fig. 7) is directly correlated with that of their precursors (Fig. 6). A coarser particle size in precursor **III** (Fig. 6c) leads to a $CuGa_2O_4$ coarse particle (Fig. 7c) while the fine homogeneous particle size from precursors **I** (Fig. 6a) and **II** (Fig. 6b) is retained in the $CuGa_2O_4$ powders (Fig. 7a and b).

The evolution of the precursor **II** at different calcined temperatures is shown in the SEM micrographs in Fig. 8. The sample calcined at 700 °C for 1 h (Fig. 8c and d) shows smaller particle size, due to the reduction of partial sintering at lower calcination temperature.

The EDX elemental analysis of the powder obtained from the precursor **II** (Fig. 8e) shows the absence of carbon, only Cu, Ga, and O were detected, with Cu:Ga:O ratios of 1:2:4. These data are in agreement with XRD

Table 3
Lattice parameter and crystallite size.

Complex precursors	Spinel phase	Lattice parameter a (Å)	Crystallite size (Å)
$(NH_4)_4[CuGa_2(C_4O_6H_4)_4(OH)_4]\cdot 5H_2O$	$CuGa_2O_4$	8.2969(5)	277.7
$(NH_4)_2[CuGa_2(C_6O_7H_{11})_4(OH)_6]\cdot H_2O$	$CuGa_2O_4$	8.2945(4)	286.2
$[CuGa_2(NH_2CH_2COO)_4(OH)_3](NO_3)\cdot 8H_2O$	$CuGa_2O_4$	8.2985(4)	291.2
$[CuGa_2(NH_2CH_2COOH)_{4.5}](NO_3)_8\cdot 6H_2O$	$CuGa_2O_4$	8.2959(4)	283.1

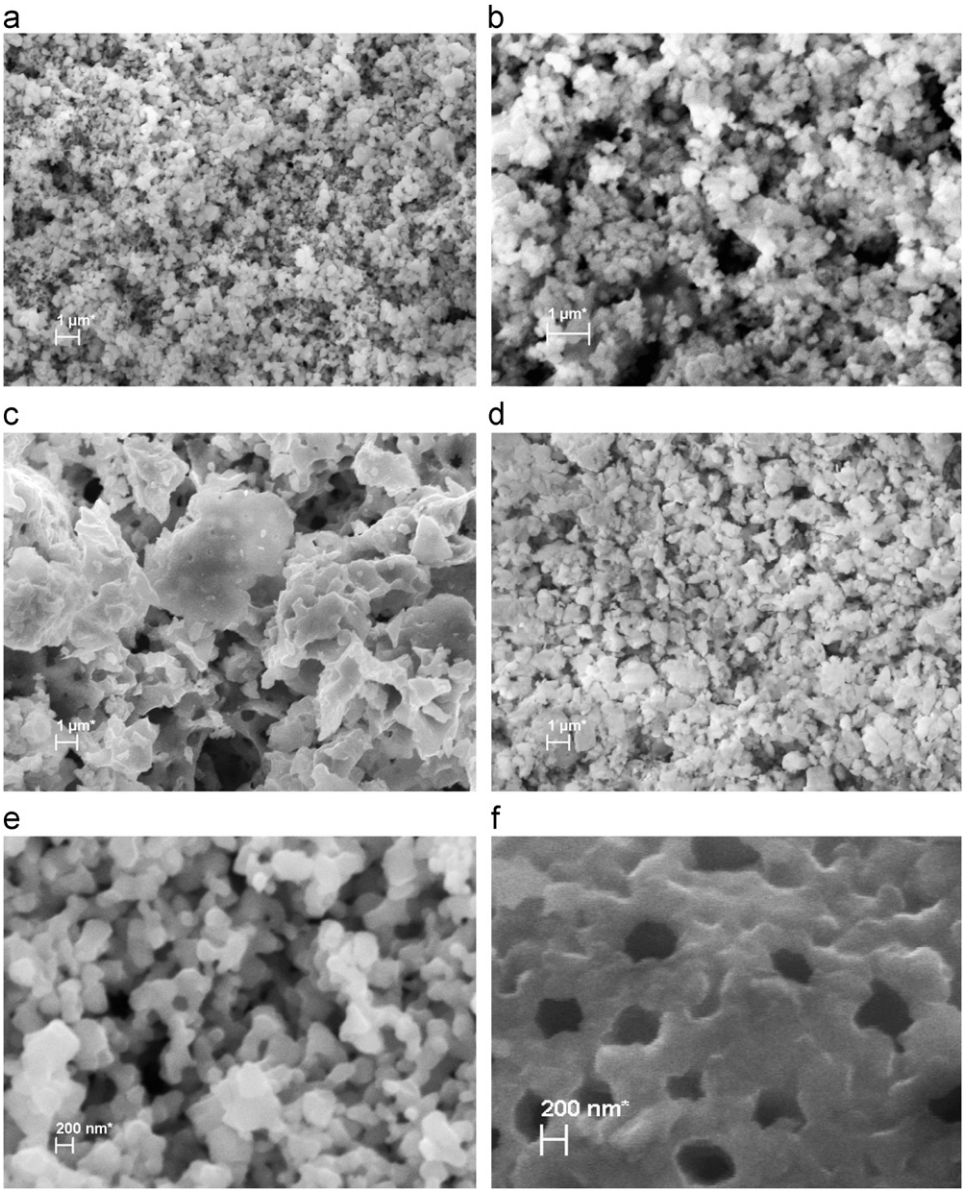

Fig. 7. SEM micrographs of $CuGa_2O_4$ samples obtained from different complex precursors: (a, e) **I**; (b) **II**; (c, f) **III** and (d) **IV**, calcined at 1000 °C for 1 h.

results and demonstrate that the Cu:Ga ratio detected in the precursor is kept unchanged in all calcined precursors, and confirm that the decomposition of the complex precursor into oxide is complete at 700 °C.

To confirm the formation of the spinel phase, the IR spectra of oxide powder samples were recorded between 4000 and 400 cm^{-1} (Fig. 9). The bands correspond to the formation of $CuGa_2O_4$ spinel [30–32].

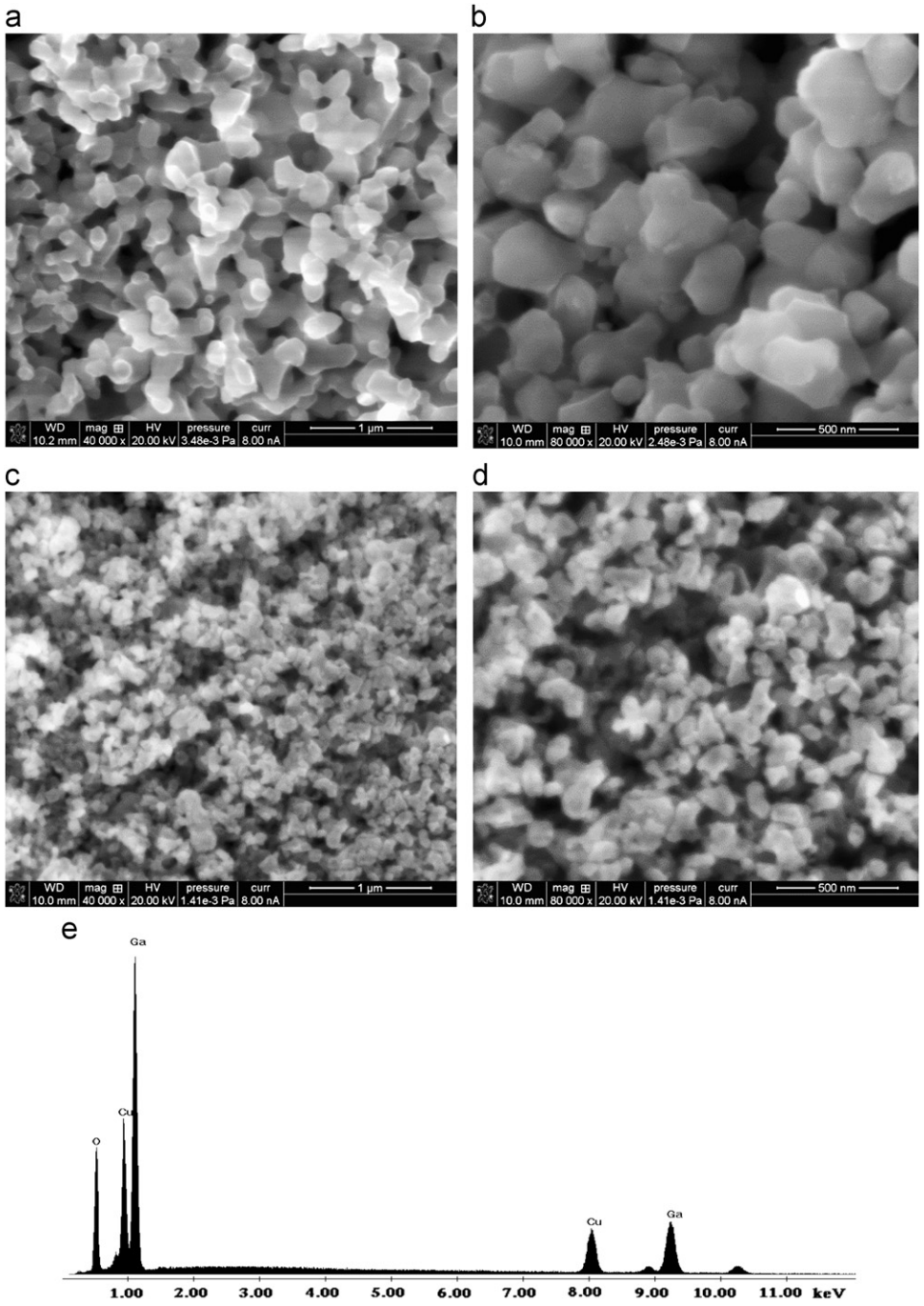

Fig. 8. SEM micrographs of $CuGa_2O_4$ obtained from complex precursor **II**: (a, b) calcined at 1000 °C for 1 h; (c, d) calcined at 700 °C for 1 h and (e) EDX spectrum of the powder calcined at 700 °C for 1 h.

The UV–vis spectra of $CuGa_2O_4$ oxides are very similar (Fig. 10). The most intensive bands which appear in the range 200–450 nm are undoubtedly charge transfer ($O \rightarrow Cu$) in origin. The other two bands centered at ~800 nm and 1600 nm are assigned to d–d transitions suggesting a distorted octahedral geometry around Cu^{2+} ions. The room temperature magnetic moments obtained for $CuGa_2O_4$ oxides $\mu_{eff} \sim 1.63–1.65$ BM smaller than μ_{theor} Cu(II) octahedral ~1.73–2.2 BM suggest the possibility of antiferromagnetic coupling between metal centers [25].

The X-band EPR spectra of $CuGa_2O_4$ obtained by thermal decomposition of **I** were recorded at 5 and 298 K (Fig. 11a). They indicate the presence of a single type of Cu-centers with $g_{II}=2.34$, $g_{\perp}=2.13$, $A_{II}=158$ G and $A_{\perp}=50$ G at 298 K and $g_{II}=2.34$, $g_{\perp}=2.12$, $A_{II}=148$ G and $A_{\perp}=70$ G at 5 K. These species are Cu^{2+} ions in a distorted octahedral coordination—an elongated octahedral one, most probably. The observed EPR spectra revealed g-values which are close to the ones reported in the literature [6,33] (Fig. 11a, Table 3). The exchange

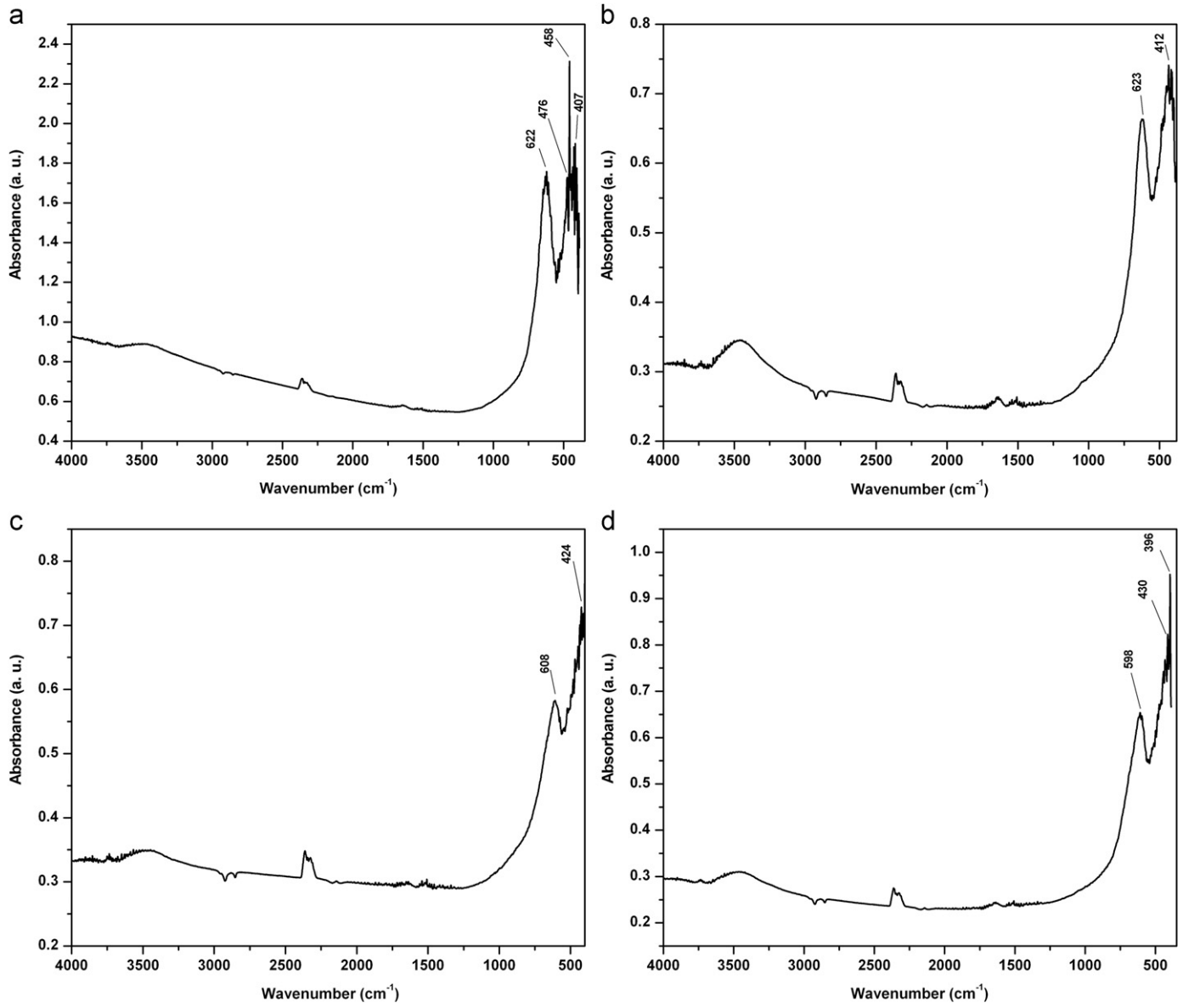

Fig. 9. IR spectra of $CuGa_2O_4$ obtained from different complex precursors: (a) **I**; (b) **II**; (c) **III** and (d) **IV**, calcined at 1000 °C for 1 h.

interaction factor $G \sim 2.83$ indicates the existence of exchange interaction between Cu centers in the oxide matrix.

The room temperature X-band EPR spectrum of $CuGa_2O_4$ obtained by thermal decomposition of **II** (Fig. 11b) is also characterized by an axial g tensor ($g_{II}=2.30$, $g_{\perp}=2.145$). Hyperfine features due to copper ($I=3/2$) could not be resolved at this temperature, suggesting that stronger interaction between metal centers might possibly occur. Indeed, calculation of the exchange interaction factor gave $G=2.07$, which is much smaller than that of $CuGa_2O_4$ obtained by thermal decomposition of **I**. At 5 K, a rhombic EPR spectrum was obtained, whose simulation lead to $g_{xx}=2.20$, $g_{yy}=1.99$ and $g_{zz}=2.27$, with $A_{xx}=A_{yy}=20$ G and $A_{zz}=230$ G (Fig. 11 b). This signal suggests a low-symmetry coordination environment around copper(II). This may be explained by the existence of defects in the matrix lattice, and/or superposition of spectra due to two different types of Cu^{2+} ions, such as hexa- and penta-coordinate species.

4. Conclusions

Copper-gallate nanoparticles were synthesized *via* two soft chemical methods: precursor method and self-propagating combustion.

The X-ray diffraction patterns of the copper gallate obtained by decomposition of the precursors **I**, **II**, and **IV** showed single phase spinelic structure. The crystallite size was about 280 Å. SEM images of $CuGa_2O_4$ obtained from complex precursors **I**–**III** evidenced that the initial morphologies of the respective precursors were held on the oxide particles.

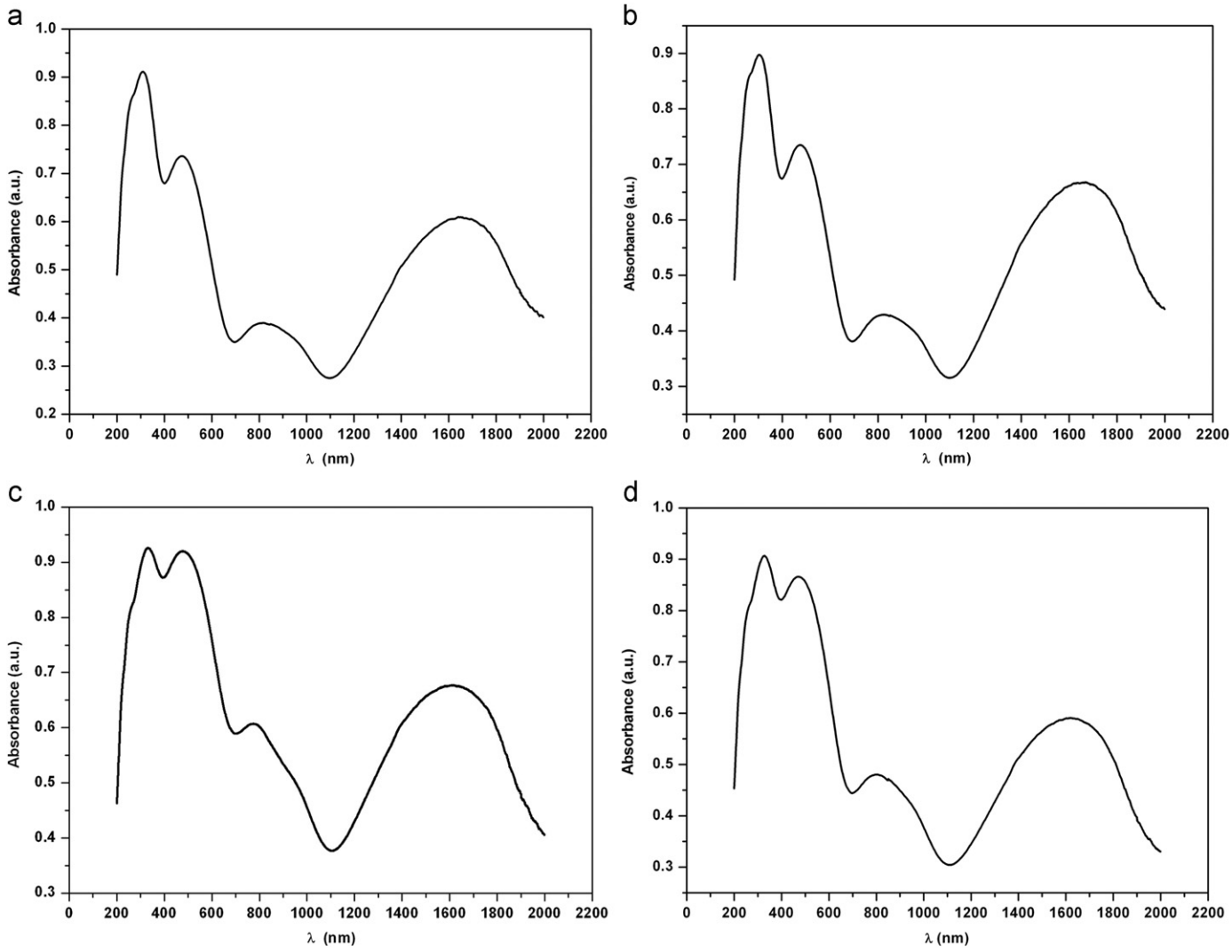

Fig. 10. UV–vis spectra of $CuGa_2O_4$ obtained from different complex precursors: (a) **I**; (b) **II**; (c) **III** and (d) **IV**, calcined at 1000 °C for 1 h.

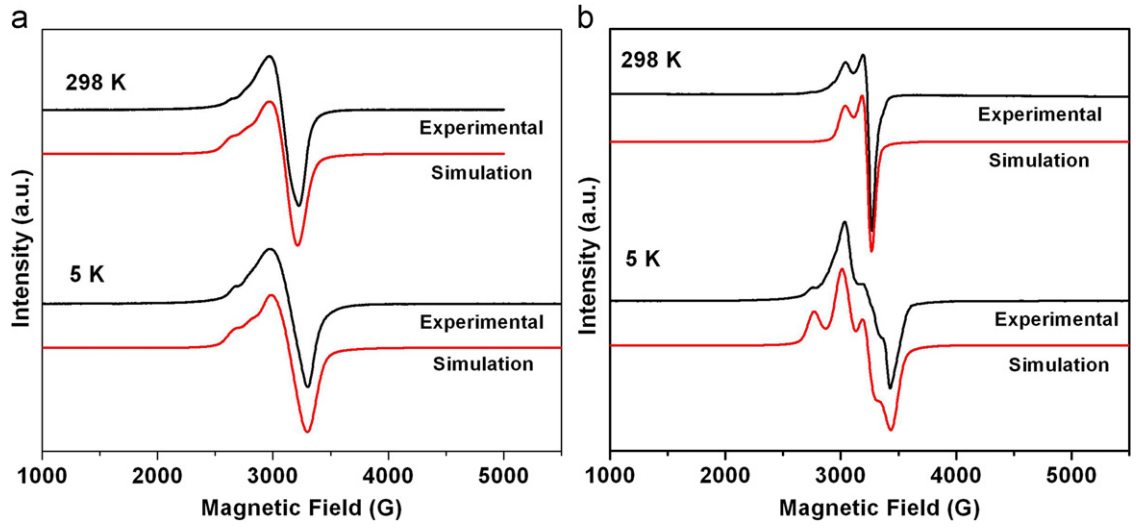

Fig. 11. X-band EPR spectra of $CuGa_2O_4$ obtained from complex precursors: (a) **I** and (b) **II**, calcined at 1000 °C for 1 h.

These results recommend the use of these two wet chemical routes for obtaining mixed oxide nanoparticles. The complex precursors containing all metal ions in the same molecule lead by thermal decomposition/self-combustion at more homogeneous mixed oxides.

Acknowledgments

This work was supported by the "Coordination and Supramolecular Chemistry" Programme of the "Ilie Murgulescu" Institute of Physical Chemistry, financed by the Romanian Academy.

References

[1] K. Faungnawakij, N. Shimoda, T. Fukunaga, R. Kikuchi, K. Eguchi, Cu-based spinel catalysts CuB_2O_4 (B=Fe, Mn, Cr, Ga, Al, $Fe_{0.75}Mn_{0.25}$) for steam reforming of dimethyl ether, Applied Catalysis A 341 (2008) 139–145.

[2] K. Gurunathan, J.O. Baeg, S.M. Lee, E. Subramanian, S.J. Moon, K. Kong, Visible light active pristine and Fe^{3+} doped $CuGa_2O_4$ spinel photocatalysts for solar hydrogen production, International Journal of Hydrogen Energy 33 (2008) 2646–2652.

[3] L. Satyanarayana, C.V. Gopal Reddy, S.V. Manorama, V.J. Rao, Liquid–petroleum–gas sensor based on a spinel semiconductor, $ZnGa_2O_4$, Sensors and Actuators B: Chemical 46 (1998) 1–7.

[4] J. Wen, X. Ge, X. Liu, Preparation of spinel-type $Cd_{1-x}Mg_xGa_2O_4$ gas-sensing material by sol–gel method, Sensors and Actuators B: Chemical 115 (2006) 622–625.

[5] S.K. Biswas, A. Sarkar, A. Pathak, P. Pramanik, Studies on the sensing behaviour of nanocrystalline $CuGa_2O_4$ towards hydrogen, liquefied petroleum gas and ammonia, Talanta 81 (2010) 1607–1612.

[6] F. Conrad, Y. Zhou, M. Yulikov, K. Hametner, S. Weyeneth, G. Jeschke, D. Günther, J.D. Grunwaldt, G.R. Patzke, Microwave-hydrothermal synthesis of nanostructured zinc–copper gallates, European Journal of Chemistry 2010 (2010) 2036–2043.

[7] Y.S. Jeong, J.S. Kim, H.L. Park, First applicability of $ZnGa_2O_4$:Ge^{4+}, Li^+, Mn^{2+} phosphor for a plasma display panel, Solid State Communications 139 (2006) 157–160.

[8] X. Chen, H. Xue, Z. Li, L. Wu, X. Wang, X. Fu, Ternary Wide Band, Gap p-block metal semiconductor $ZnGa_2O_4$ for photocatalytic benzene degradation, Journal of Physical Chemistry C 112 (2008) 20393–20397.

[9] U.K. Gautam, Y. Bando, J. Zhan, P.M. Costa, X.S. Fang, D. Golberg, Ga-doped ZnS nanowires as precursors for ZnO/$ZnGa_2O_4$ nanotubes, Advanced Materials 20 (2008) 810–814.

[10] S. Komarneni, H. Katsuki, Nanophase materials by a novel microwave-hydrothermal process, Pure and Applied Chemistry 74 (2002) 1537–1543.

[11] P.M. Aneesh, K.M. Krishna, M.K. Jayaraj, Hydrothermal synthesis and characterization of undoped and Eu-doped $ZnGa_2O_4$ nanoparticles, Journal of the Electrochemical Society 156 (2009) K33–K36.

[12] K. Sung, T.M. Chung, C.G. Kim, Combining thermolysis of molecular precursor with sol–gel process to zinc gallate nanoparticles, Materials Letters 61 (2007) 1011–1014.

[13] D. Gingasu, I. Mindru, G. Marinescu, L. Patron, C. Ghica, Ultrafine particles of $ZnGa_2O_4$ obtained by solution combustion and complexation methods, Journal of Alloys and Compounds 481 (2009) 890–895.

[14] A.S. Prakash, A.M.A. Khadar, K.C. Patil, M.S. Hegde, Hexamethylenetetramine: a new fuel for solution combustion synthesis of complex metal oxides, Journal of Materials Synthesis and Processing 10 (2002) 135–141.

[15] S.R. Jain, K.C. Adiga, V.R. Pai Verneker, A new approach to thermochemical calculations of condensed fuel-oxidizer mixtures, Combustion and Flame 40 (1981) 71–79.

[16] R.C. Kambale, P.A. Shaikh, N.S. Harale, V.A. Bilur, Y.D. Kolekar, C.H. Bhosale, K.Y. Rajpure, Structural and magnetic properties of $Co_{1-x}Mn_xFe_2O_4$ ($0 \le x \le 0.4$) spinel ferrites synthesized by combustion route, Journal of Alloys and Compounds 490 (2010) 568–571.

[17] J. Livage, Vanadium pentoxide gels, Chemistry of Materials 3 (1991) 578–593.

[18] J. Livage, M. Henry, C. Sanchez, Sol–gel chemistry of transition metal oxides, Progress in Solid State Chemistry 18 (1988) 259–341.

[19] D. Avnir, T. Coradin, O. Lev, J. Livage, Recent bio-applications of sol–gel materials, Journal of Materials Chemistry 16 (2006) 1013–1030.

[20] C. Sanchez, L. Rozes, F. Ribot, C. Laberty-Robert, D. Grosso, C. Sassoye, C. Boissiere, L. Nicole, Chimie douce: a land of opportunities for the designed construction of functional inorganic and hybrid organic–inorganic nanomaterials, Comptes Rendus Chimie 13 (2010) 3–39.

[21] K. Nakamoto, Infrared and Raman Spectra of Inorganic and Coordination Compounds, Wiley, New York, 1986.

[22] Y. Subba Rao, B. Prathima, S. Adinarayana Reddy, K. Madhavic, A. Varada Reddy, Complexes of Cu(II) and Ni(II) with bis(phenylthiosemicarbazone): synthesis, spectral, EPR and in vitro—antibacterial and antioxidant activity, Journal of the Chinese Chemical Society 57 (2010) 677–682.

[23] A. Veeraraj, P. Sami, N. Raman, Copper(II) complex of 3-cinnamalideneacetylacetone: synthesis and characterization, Proceedings of the Indian Academy of Sciences (Chemical Science) 112 (2000) 515–521.

[24] M.G. Alexandru, I. Jitaru, P. Bourosh, C. Draghici, E. Jeanneau, V. Kravtsov, Y.A. Simonov, Two new hydrogen bonded networks obtained in $MCl_2 \cdot xH_2O$ (M=Mn, Cu)-N,N′-ethylenebisacetamide system, Revue Roumaine de Chimie 54 (2009) 1119–1123.

[25] R. Carballo, B. Covelo, S. Balboa, A. Castiñeiras, J. Niclós, Mixed-ligand complexes of copper(II) with α-hydroxycarboxylic acids and 1,10-phenanthroline, Zeitschrift für Anorganische and Allgemeine Chemie 627 (2001) 948–954.

[26] S. Deshpande, D. Srinivas, P. Ratnasamy, EPR and catalytic investigation of Cu(salen) complexes encapsulated in zeolites, Journal of Catalysis 188 (1999) 261–269.

[27] F. Rafar, M.Y. Siddiqi, K.S. Siddiqi, Synthesis and characterization of Ni(II), Cu(II) and Co(III) complexes with polyamine-containing macrocycles bearing an aminoethyl pendant arm, Journal of the Serbian Chemical Society 69 (2004) 641–649.

[28] B.J. Hathaway, A.A.G. Tomlinson, Copper(II) ammonia complexes, Coordination Chemistry Reviews 5 (1970) 1–43.

[29] I.M. Procter, B.J. Hathaway, P. Nicholls, The electronic properties and stereochemistry of the copper(II) ion. Part I. Bis(ethylenediamine)copper(II) complexes, Journal of the Chemical Society A (1968) 1678–1682.

[30] J. Preudhomme, P. Tartre, Infrared studies of spinels—II. The experimental bases for solving the assignment problem, Spectrochimica Acta A 27 (1971) 845–851.

[31] J. Preudhomme, P. Tartre, Infrared studies of spinels—III: the normal II–III spinels, Spectrochimica Acta A 27 (1971) 1835–1871.

[32] I. Mindru, G. Marinescu, D. Gingasu, L. Patron, C. Ghica, M. Giurginca, Blue $CoAl_2O_4$ spinel *via* complexation method, Materials Chemistry and Physics 122 (2010) 491–497.

[33] P.K. Sharpe, J.C. Vickerman, Solid state properties of copper containing spinel solid solutions ($Cu_xMg_{1-x}Al_2O_4$), Journal of the Chemical Society Faraday Transactions I (1977) 505–513.